Multinuclear NMR study on the formation and polyol-induced deformation mechanisms of worm-like micelles composed of cetyltrimethylammonium bromide and 3-fluorophenylboronic acid

Ryotaro Miki,† Tomoya Yamauchi,† Kosuke Kawashima,† Yuya Egawa,† Toshinobu Seki,†*

†Faculty of Pharmacy and Pharmaceutical Sciences, Josai University, 1-1 Keyakidai, Sakado, Saitama 350-0295, Japan

**To whom correspondence should be addressed: Faculty of Pharmacy and Pharmaceutical Sciences, Josai University, 1-1 Keyakidai, Sakado, Saitama 350-0295, Japan*

E-mail: rmiki@josai.ac.jp

Tel: +81-49-271-7686

Fax: +81-49-271-7714

KEYWORDS: worm-like micelles, viscosity change, phenylboronic acid, polyol-responsive, multinuclear NMR

ABSTRACT

We had previously confirmed a glucose-responsive decrease in the viscosity of cetyltrimethylammonium bromide (CTAB) and phenylboronic acid (PBA) worm-like micelles (WLMs) systems. However, the mechanisms of the formation of WLMs and the decrease in viscosity with glucose addition have not been determined. In this study, we elucidated the mechanisms using 3-fluorophenylboronic acid (3FPBA) based on ^{11}B NMR and ^{19}F NMR analyses. The system in 60 mM CTAB/60 mM 3FPBA at pH 7.4 demonstrated high viscoelasticity, and the formation of WLMs in the system was confirmed by rheological characteristics. The ^{11}B NMR spectrum at pH 7.4 revealed that 3FPBA existed in a neutral form with sp^2-hybridized boron; however, the ^{11}B signal disappeared in the presence of CTAB. In contrast, ^{19}F NMR studies indicated that the quaternary ammonium ion of CTAB interacts with the phenyl group of 3FPBA in the sp^2 form via cation-π interactions. PBA derivatives react with various polyols, thus, we investigated the change in the viscous system after the addition of sugar and sugar alcohols. The viscosity of the WLMs decreased with increased polyol concentration, especially those of fructose and mannitol, in which the decrease was apparent at 40–160 mM polyols. The ^{19}F NMR spectra revealed that polyol addition induced decrease in the sp^2 form of 3FPBA and increase in the sp^3 form of 3FPBA. Based on the results, we propose the following mechanism of the polyol response. (1) The WLMs are stabilized by CTAB and 3FPBA in the sp^2 form using cation–π interactions as the driving force. (2) When polyol is added to the system, the sp^2 form of 3FPBA decreases, and its sp^3 form increases. (3) This change means that the structural component of WLMs decreases, which induces the disruption of WLMs, and the viscosity decreases. The formation and deformation mechanisms of the WLMs determined in this study are notable because 3FPBA interacts as a neutral compound, whereas CTAB often

interacts with anionic aromatic compounds to form WLMs. Without ^{19}F NMR measurements, these mechanisms would not have been discovered.

1. INTRODUCTION

Gels are typically divided into two main categories, chemical or physical, based on the type of cross-linking[1,2]. Chemical gels are cross-linked by covalent bonds; however, once this cross-link is broken, the structure of the gel does not recover. Conversely, physical gels are cross-linked by non-covalent bonds. In physical gels, as the cross-link is broken, the material reforms and completely recovers owing to its viscoelasticity. Several types of physical gels consist of low-molecular-weight compounds, which are assembled by intermolecular interactions[3–5]. In some of these molecular assemblies, the structures can be changed drastically by external stimuli. Worm-like micelles (WLMs) form sterically entangled networks that are produced by molecular interactions between surfactants and aromatic compounds. These WLMs exhibit unique and remarkable viscoelastic behavior[6,7]. Several stimuli-responsive WLMs[8] have been reported, such as light[9–12], thermal change[13], redox[14,15], and pH change[16]. Given the considerations and advantages mentioned above, these smart WLMs are potentially applicable to a wide range of fields.

In the pharmaceutical field, sugar-responsive smart materials are required for diabetes mellitus. Hyperglycemia can result in severe health complications over time in patients with diabetes mellitus. Insulin administration and measurement of blood glucose (Glc) levels are essential for the therapeutic management of diabetes mellitus. Sugar-responsive smart materials, particularly those that are Glc-responsive, are promising controlled-release systems for hyperglycemia[17,18] or

in analytical chemistry applications for blood Glc levels[19]. Many of these sugar-responsive materials utilize phenylboronic acid (PBA; **Figure 1a**) derivatives as sugar-sensing moiety[18–21]. PBA is a Lewis acid; a hydroxide ion reversibly coordinates with boron to form a boronate anion at higher pH, changing the hybridization state of boron from sp^2 to sp^3. This change is regarded as an acid-base equilibrium and can be described using pK_a. The phenylboronate anion reversibly forms a cyclic ester with the *cis*-diol moieties of polyol (**Figure 1d**).

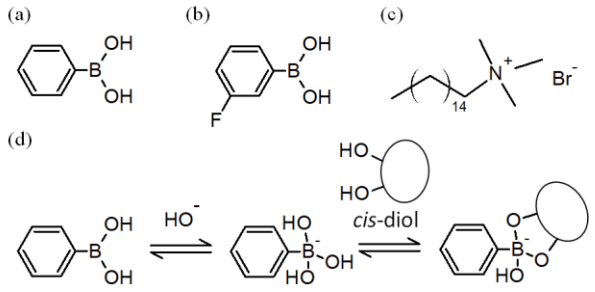

Figure 1. Chemical structures of (a) phenylboronic acid (PBA), (b) 3-fluorophenylboronic acid (3FPBA), (c) cetyltrimethylammonium bromide (CTAB), and (d) acid-base equilibrium of PBA and the binding equilibrium between PBA and *cis*-diol compounds.

Hydrogels containing PBA derivatives have potential for H_2O_2-triggered release systems[22,23] and saccharide assays[24,25]. We previously reported a novel Glc-responsive WLM consisting of cetyltrimethylammonium bromide (CTAB; **Figure 1c**) and PBA[26]. In the absence of Glc, the micelle behaves in a gel-like manner; however, when Glc is added, the viscosity decreases. The mechanism of formation of WLMs and the decrease in viscosity with Glc have not been elucidated. It is necessary to study the intermolecular interactions or hybridization states of the

boron in PBA to clarify this mechanism. Generally, ^{11}B NMR spectroscopy is useful for these studies. In addition, for PBA derivatives with fluorine, the hybridization state of boron can be determined by ^{19}F NMR analysis. London et al. successfully obtained the pK_a of 4-fluorophenylboronic acid by ^{19}F NMR analysis [27]. In this study, we prepared CTAB-based WLMs using 3-fluorophenylboronic acid (3FPBA; **Figure 1b**) instead of PBA to investigate both ^{11}B and ^{19}F NMR spectra. Moreover, we studied the polyol response of the WLMs and its response mechanism. We described the system by visual observation, rheological measurements, ultraviolet (UV) spectroscopy, ^{1}H NMR, ^{11}B NMR and ^{19}F NMR.

2. EXPERIMENTAL SECTION

2.1. Materials

Sodium tetrafluoroborate ($NaBF_4$), galactose (Gal), pentaerythritol (Pen), and 3FPBA were obtained from Tokyo Chemical Industry (Tokyo, Japan). Glc, fructose (Fru), mannitol (Man), diethylene glycol (DEG), sodium hydroxide solution (1 mol/L), CTAB, sodium chloride (NaCl), and trifluoroacetic acid (TFA) were obtained from FUJIFILM Wako Pure Chemical Co. (Osaka, Japan). Deuterium oxide (D_2O) was purchased from Kanto Chemical Co. Inc. (Tokyo, Japan). Solutions of sodium deuteroxide (NaOD) (40% (w/w)) and deuterium chloride (DCl) (35% (w/w)) were acquired from Sigma-Aldrich (Tokyo, Japan).

2.2. Preparation of the CTAB/3FPBA mixed system

CTAB and 3FPBA were dissolved in distilled water to obtain the desired concentration. Aqueous NaOH solution was used to adjust the pH. After mixing the system at 37 °C for more than 12 h, the prepared systems were maintained at 25 °C for more than 24 h to achieve equilibrium.

2.3. Observation of appearance

Aliquots of the prepared solutions (2.0 mL) were transferred into 6-mL glass vials. Images were obtained 20 s after reversing the vials.

2.4. Rheological measurements

Steady and dynamic rheological measurements were conducted at 25 °C using a stress-controlled rotational rheometer (MCR-102; Anton Paar, Ostfildern, Germany). A cone plate or concentric cylinder was used for both measurements. The strain (γ) was fixed at 10% when monitoring the dynamic viscoelasticity.

2.5. UV spectroscopy

The UV absorption spectra were recorded using a JASCO V-560 spectrometer (JASCO Corporation, Tokyo, Japan).

2.6. NMR measurements

A Varian 400-MR spectrometer (Agilent Technologies, CA, USA) was used for the NMR analyses. $NaBF_4$ or TFA was used as the external standard for ^{11}B NMR or ^{19}F NMR, respectively, and their chemical shifts (δ) were set to 0 ppm. In the ^{11}B or ^{19}F NMR, a 10% aqueous D_2O solution was used as the solvent, and the error in the pH was assumed to be negligible. Thus, the pH values were recorded directly from the pH meter. The concentration of 3FPBA was fixed at 10 mM. In the presence of CTAB, the concentration of CTAB was fixed at 10 mM. For the ^1H NMR measurements, the pD values were obtained by converting the apparent pH values measured in D_2O using the following equation[28,29]:

$$pD = \text{apparent pH} + 0.44 \qquad (1)$$

NaOD or DCl solutions were used to adjust the pD. In all NMR studies, the viscosity of the solution was sufficiently low to facilitate the measurement of the solution NMR spectra.

3. RESULTS AND DISCUSSION

3.1. Preparation of the gel and its Glc response

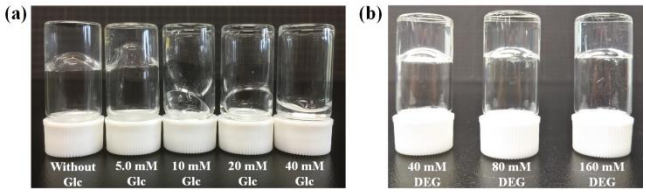

Figure 2. Photographs of System 1 with various concentrations of (a) Glc or (b) diethylene glycol (DEG).

We observed a formulation comprising 60 mM CTAB and 60 mM 3FPBA (System 1) at pH 7.4, with or without different concentrations of Glc (**Figure 2a**). System 1 without Glc exhibited a gel-like appearance. When the Glc concentration of System 1 was more than 10 mM, the gel exhibited a sol-like appearance. These results confirmed that System 1 exhibited Glc-responsiveness. We successfully prepared a new CTAB/3FPBA viscous system whose viscosity decreases with increasing Glc concentration. We used DEG as a control diol compound because it does not react with boronic acid. System 1, with 40–160 mM DEG, maintained a gel-like appearance (**Figure 2b**).

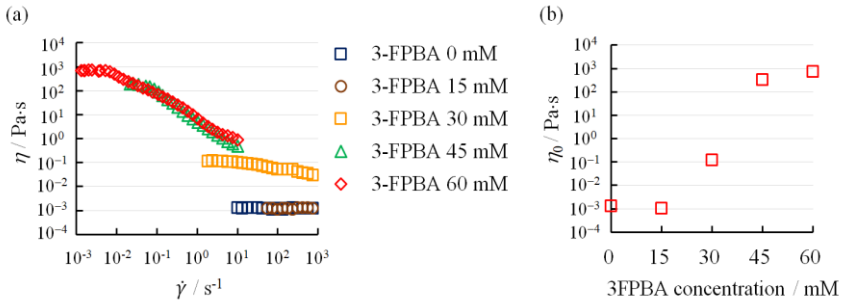

Figure 3. (a) Steady shear rate ($\dot{\gamma}$)-dependent viscosity (η) behaviors in various 3-fluorophenylboronic acid (3FPBA) concentrations with 60 mM cetyltrimethylammonium bromide (CTAB) at pH 7.4, (b) Relationship between 3FPBA concentration and η_0 with 60 mM CTAB at pH 7.4.

We performed steady-state viscosity measurements to investigate the effects of the temperature, pH, and concentration of 3FPBA as well as the addition of NaCl, Glc, or DEG on the viscosity. **Figure 3a** depicts the viscosity (η) behavior as a function of the shear rate ($\dot{\gamma}$) in a formulation with a fixed CTAB concentration (60 mM) and various 3FPBA concentrations at pH 7.4.

The zero-shear viscosity (η_0) was obtained from the extrapolation of η, which demonstrates a similar value that is independent of $\dot{\gamma}$ on the y-axis. In 60 mM 3FPBA, η was almost constant at lower $\dot{\gamma}$; however, η decreased as $\dot{\gamma}$ increased beyond a certain value. This result means that the structure of the system is maintained until a certain shear rate, but breaks thereafter. These characteristic rheological properties are observed in typical WLMs[30,31]. **Figure 3b** shows the relationship between the 3FPBA concentration and η_0. The η_0 increases as the 3FPBA concentration increases from 1.3 mPa·s (without 3FPBA) to 717.0 Pa·s (with 60 mM 3FPBA). This difference corresponds to a factor of 10^6. The η_0 value without 3FPBA is close to that of distilled water (0.91 mPa·s) (**Figure S1**).

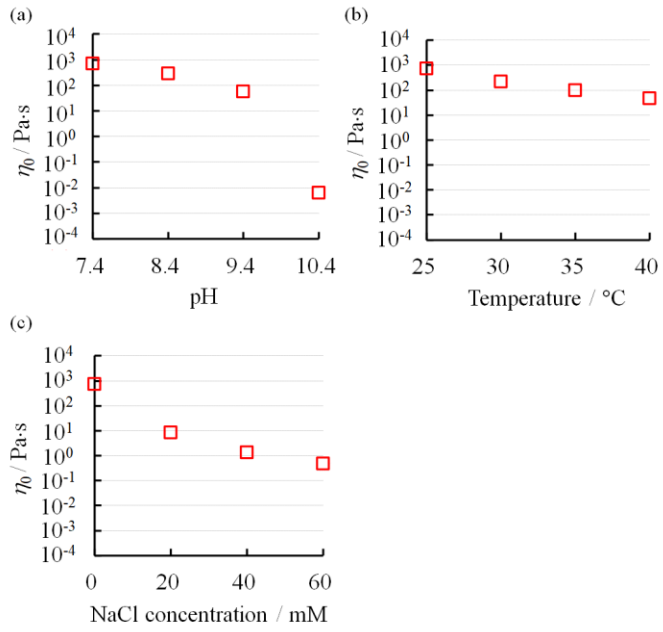

Figure 4. Dependence of the zero-shear viscosity (η_0) of System 1 (60 mM cetyltrimethylammonium bromide and 60 mM 3-fluorophenylboronic acid) at different (a) pH levels, (b) temperatures at pH 7.4, and (c) NaCl concentrations at pH 7.4.

Figure 4a presents the relationship between the pH and η_0 for System 1. As the pH increased from 7.4 to 10.4, η_0 decreased from 717.0 Pa·s to 6.43 mPa·s. The pK_a of 3FPBA was 8.5 (see section 3.3), which indicated that 3FPBA mainly existed in anionic form at pH 10.4. Therefore, we hypothesized that the high η_0 of System 1 was caused by the interactions between CTAB and neutral 3FPBA but not anionic 3FPBA. The results of the experiment in which Glc was added to System 1 (**Figure 2a**) also supported this hypothesis: Glc converted neutral 3FPBA to the anionic sugar-bound form of 3FPBA, which caused the viscosity to decrease.

Figure 4b illustrates the relationship between the temperature and η_0 for System 1 at pH 7.4. As the temperature increased from 25 to 40 °C, η_0 decreased from 717.0 to 46.2 Pa·s. This trend is typical for micellar solutions comprising cationic surfactants and anionic aromatic compounds[32]. **Figure 4c** depicts the relationship between the NaCl concentration and η_0 for System 1 at pH 7.4. As the NaCl concentration increased from 0 to 60 mM, η_0 decreased from 717.0 Pa·s to 479.5 mPa·s. Typically, the addition of excess salt disrupts the WLMs of systems that contain ionic surfactants and decreases their viscosity[33].

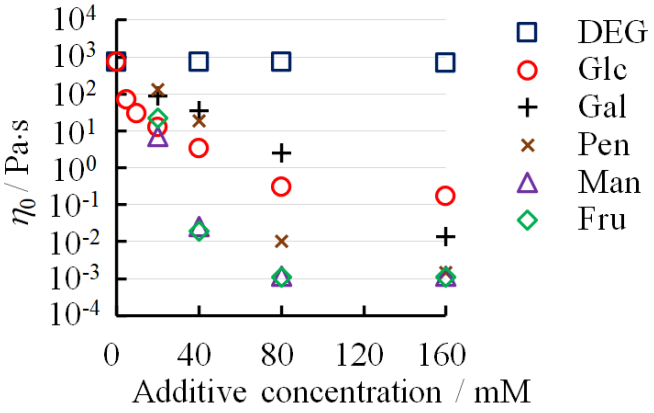

Figure 5. The behavior of η_0 with various concentrations of polyols in System 1 at pH 7.4.

PBA derivatives react with various polyols[34], which explains the change in viscosity of System 1 in the presence of sugar or sugar alcohol. **Figure 5** shows the variation in the η_0 of System 1 at pH 7.4 as a function of polyol concentration. As the effect of polyols in the range 20–80 mM was

indeterminate. Contrary to expectations, η_0 for Fru was higher than that of Man and Glc at 20 mM polyol concentration. It is well known that Glc and Gal can react with two PBAs because they have two binding sites for PBA, viz. α-D-glucofuranose and α-D-galactofuranose[35]. Pen can also react with two PBAs[36]. Multiple interactions might be a factor in the unexpected results obtained in the polyol concentration range 20–80 mM, as shown in Fig. 5. At 40 mM polyol concentration, η_0 for Fru (19.1 mPa·s) was similar to that for Man (25.8 mPa·s). This result indicates that the binding constant of Fru to PBA (160 M^{-1}) is similar to that of Man (120 M^{-1}). At 80 mM polyol concentration, η_0 for Fru and Man were almost 1 mPa·s, equal to that of water and spherical micelle solutions[26]. Thus, η_0 values of Fru and Man do not decrease at concentrations greater than 80 mM. Instead of considering the aforementioned complex results, we focused on the effect of 160 mM polyols. The polyols' effect on η_0 follows the order Fru, Man > Pen > Gal > Glc > DEG. This trend bears close correlation to polyol reactivity with PBA[34,37]. The difference in η_0 between the system without polyols and that with 160 mM Fru corresponds to approximately $1/10^6$. By contrast, the effect of DEG on η_0 was negligible; η_0 was 680.0–751.9 Pa·s with 0–160 mM DEG, which agrees with the fact that DEG does not bind with PBA derivatives. From the results of various parameters on η_0, we confirmed that System 1 shows reactivity to polyols by reflecting the reactivity of PBA derivatives.

3.2. Investigation of the formation of the WLM structure using dynamic viscoelasticity measurements

We measured dynamic viscoelasticity to obtain additional information on the rheological properties and to investigate the formation or deformation of the WLMs in System 1. We monitored the behaviors of both the storage modulus (G') and loss modulus (G'') at different

frequencies (ω). G' and G'' correspond to the elasticity and viscosity, respectively. These two parameters are based on the Maxwell model in Eqs. (2) and (3).

$$G' = \frac{\omega^2\tau^2}{1+\omega^2\tau^2} \cdot G_0 \qquad (2)$$

$$G'' = \frac{\omega\tau}{1+\omega^2\tau^2} \cdot G_0 \qquad (3)$$

where G_0 and τ are the plateau modulus and relaxation time, respectively. When the rheological character that fits the Maxwell model has a single τ, G' and G'' can produce a semicircular shape in the Cole-Cole plot (G' versus G''), which is shown in Eq. (4)[6,38].

$$\left(G' - \frac{G_0}{2}\right)^2 + G''^2 = \frac{G_0^2}{4} \qquad (4)$$

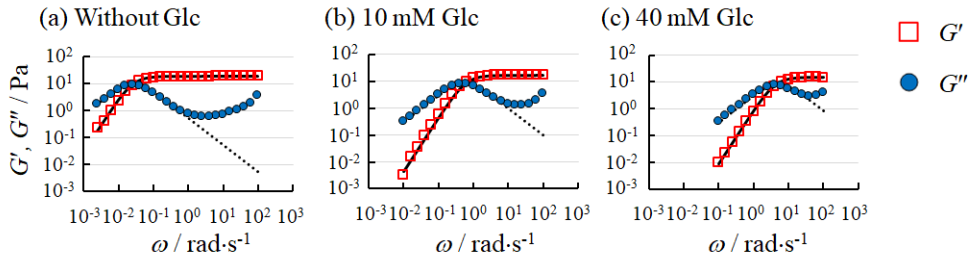

Figure 6. The frequency-dependent behaviors of storage modulus (G') and loss modulus (G'') with different Glc concentrations at pH 7.4. The dotted and solid curve fittings were calculated according to Eq. 2 and 3, respectively.

Figure 6 shows the frequency-dependent behaviors of G' and G'' in System 1 at pH 7.4. The profiles of G' without Glc follow the simple Maxwell model shown in Eq. 2. The profiles of G' and G'' without Glc differ from those with 10 or 40 mM Glc.

The Cole-Cole plot is useful to determine how well the data fits the Maxwell model with a single τ[6,38]. The Cole-Cole plots were used to confirm the presence of WLMs[30,39,40]. **Figure S2** shows the Cole-Cole plots in System 1 based on the results of **Figure 6a**, **c**.

In the absence of Glc, a typical semicircular shape is observed (**Figure S2a**). Typical WLMs portray a semicircular Cole-Cole plot, which explains the rheological character and reflects the single Maxwell model with a single τ[6,41]. Therefore, we determined that at pH 7.4, System 1 forms WLMs. In contrast, in the presence of 40 mM Glc, the shape of the semicircle is slightly deformed (**Figure S2b**). This result suggests that the WLM structure is partially broken.

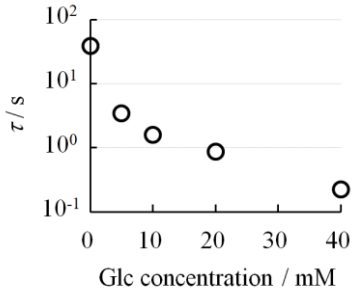

Figure 7. The behavior of relaxation time (τ) at various concentrations of Glc in System 1 at pH 7.4.

To further investigate the effect of Glc on the deformation of WLMs, we evaluated τ from the results of dynamic viscoelasticity. We obtained the ω_c at which G' and G'' are equal. The ω_c (intersection between G' and G'') shifts higher with increasing Glc concentrations (**Figure 6**). Then, we estimated τ according to $1/\omega_c$. The parameter τ provides information on the WLM length because a higher τ indicates the formation of highly entangled WLMs[30,42]. **Figure 7** shows the behavior of τ at various concentrations of Glc.

An increase in the Glc concentration from 0 to 40 mM lowered τ. This result demonstrates that Glc breaks the chains of the WLMs to make them shorter[30,42], which is related to the partial disintegration of the WLMs.

3.3. pK_a measurements for 3FPBA

From the macroscopic scale point-of-view, we understand the polyol-responsive behavior of the WLMs; the viscosity of System 1 decreases by adding polyol. From the molecular-level point-of-view, the pK_a of 3FPBA helps us understand the sp^2/sp^3 hybridization state of boron in 3FPBA. We measured the UV spectra at different pH values (**Figure S3**) to obtain the pK_a of 3FPBA. From the relationship between pH and absorbance at 268 nm, the pK_a of 3FPBA is calculated to be 8.4 by using curve fitting analysis[34] (**Figure S4**).

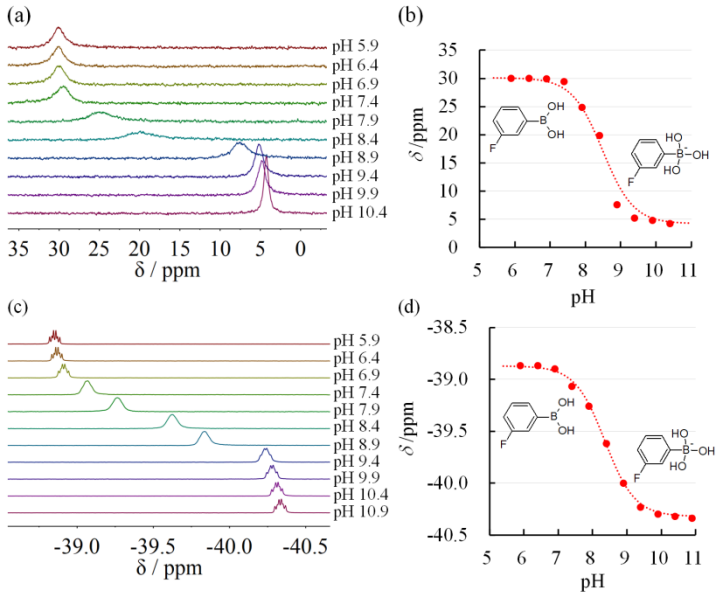

Figure 8. (a) ^{11}B NMR spectra of 3-fluorophenylboronic acid (3FPBA; 10 mM) in 10% (v/v) aqueous D_2O solution at different pH levels and (b) changes in δ of 3FPBA with the pH. (c) ^{19}F NMR spectra of 3FPBA (10 mM) in 10% (v/v) aqueous D_2O solution at different pH values and (d) changes in δ of 3FPBA with the pH.

We measured the ^{11}B NMR and ^{19}F NMR spectra to study the hybridization state of sp^2/sp^3 boron in 3FPBA. For this purpose, ^{19}F NMR for boronic acid-containing F is a powerful tool[27,43–45].

Figure 8 presents the ^{11}B NMR and ^{19}F NMR spectra of 10 mM 3FPBA at different pH values and the variation in δ of 3FPBA, respectively. The pK_a of 3FPBA is calculated to be 8.5 from both curve fittings (**Figures 8b** and **d**). This pK_a value is close to pK_a 8.4, which is obtained from the UV spectra (**Figure S4**); therefore, the values are reasonable. From the pK_a value of 8.5, we conclude that 3FPBA is present in a neutral form with an sp^2 hybridized boron at pH 7.4.

3.4. Study of the behavior of 3FPBA with/without CTAB or polyol

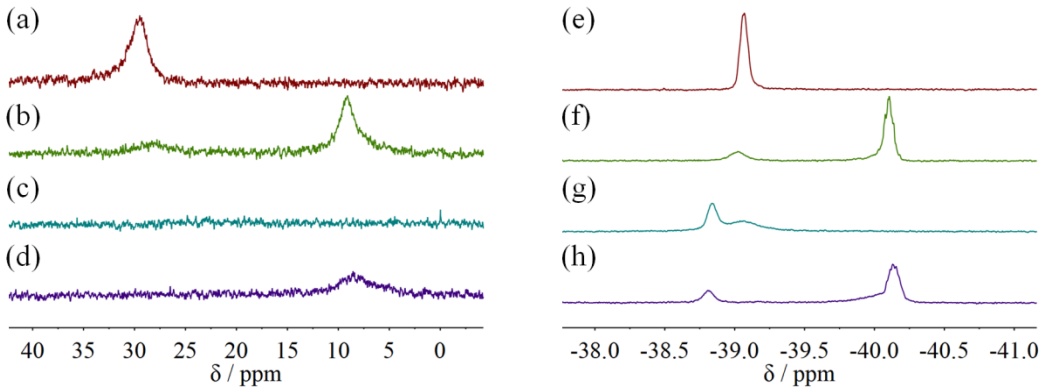

Figure 9. (a)–(d) ^{11}B NMR spectra of 10 mM 3-fluorophenylboronic acid (3FPBA) in 10% (v/v) aqueous D_2O solution at pH 7.4 (a) without cetyltrimethylammonium bromide (CTAB) or Glc, (b) with 200 mM Glc, (c) with 10 mM CTAB, and (d) with 10 mM CTAB and 200 mM Glc. (e)–(h) ^{19}F NMR spectra of 10 mM 3FPBA in 10% (v/v) aqueous D_2O solution at pH 7.4 (e) without CTAB or Glc, (f) with 200 mM Glc, (g) with 10 mM CTAB, and (h) with 10 mM CTAB and 200 mM Glc.

We further assessed the ^{11}B NMR and ^{19}F NMR spectra to determine the intermolecular interactions of 3FPBA. **Figure 9** depict the ^{11}B NMR and ^{19}F NMR spectra of 3FPBA at pH 7.4 with/without CTAB or Glc, respectively. In the ^{11}B NMR of 3FPBA without CTAB or Glc, a single signal is observed at 29.5 ppm (**Figure 9a**). This signal is mainly derived from the sp^2

boron[46]. Under the same conditions in the ^{19}F NMR, a single signal is observed at −39.1 ppm (**Figure 9e**). This signal is also mainly derived from the sp^2 boron[27].

In the presence of 200 mM Glc, new signals appear at 9.1 ppm in ^{11}B NMR (**Figure 9b**) and at −40.2 ppm in ^{19}F NMR (**Figure 9f**). These signals are derived from the sp^3 boron[27,46].

Unfortunately, the presence of 10 mM CTAB induces the disappearance of the ^{11}B signal of 3FPBA (**Figure 9c**). Although the reason for this is unclear, it might be due to the low sensitivity of ^{11}B because the spin quantum number of ^{11}B is 3/2. In contrast, under identical conditions in ^{19}F NMR, a single signal is detected, which exhibits a downfield shift from −39.1 ppm (**Figure 9e**) to −38.8 ppm (**Figure 9g**). The detectability of ^{19}F NMR is higher than that of ^{11}B NMR because the spin quantum number of ^{19}F is 1/2. This difference is one of the factors enabling ^{19}F NMR to detect signals in the presence of 10 mM CTAB. Similar downfield shifts in **Figure 9g** have been reported in fluorobenzene derivatives/cationic surfactant systems[47,48]. The downfield shift in **Figure 9g** suggests that the electron density near the aromatic ring decreases.

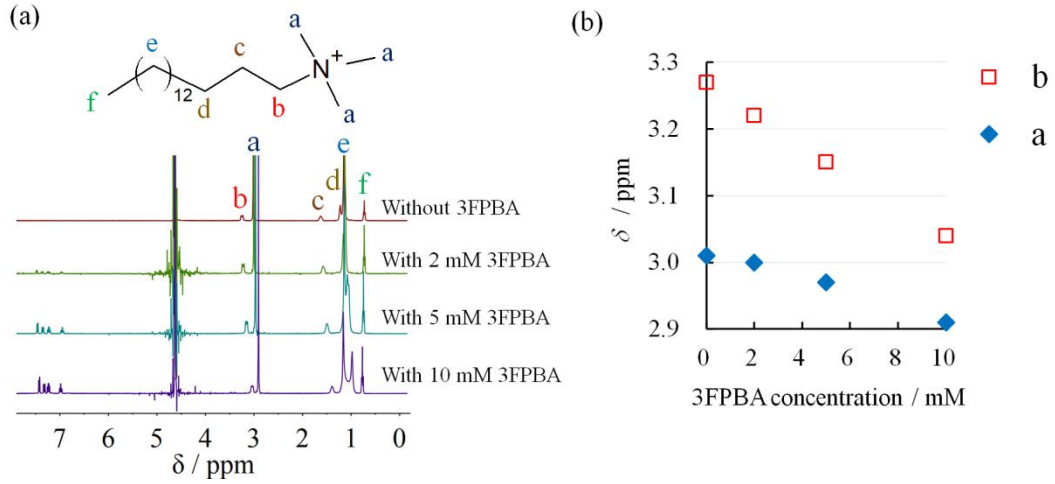

Figure 10. (a) ^{1}H NMR spectra of cetyltrimethylammonium bromide (10 mM) with different concentrations of 3-fluorophenylboronic acid (3FPBA) in D_2O at pD 5.8 and (b) changes in δ_a and δ_b with the 3FPBA concentration.

To support this hypothesis, we obtained the ^{1}H NMR spectra of CTAB and 3FPBA mixtures at pD 5.8, at which 3FPBA exists in neutral form. **Figure 10a** illustrates the ^{1}H NMR spectra of 10 mM CTAB with different 3FPBA concentrations, and **Figure 10b** depicts the changes in δ_a and δ_b around the ammonium groups of CTAB with the 3FPBA concentration. The increase in 3FPBA concentration caused δ_a and δ_b to shift upfield, which suggested that the electron density around the quaternary ammonium groups of CTAB increased. Similar upfield shifts have been reported when CTAB and the phenyl groups of aromatic compounds interacted via cation-π interactions[16,49,50]. From the results in **Figures 9e and g and 10**, we propose that the quaternary ammonium ion of CTAB interacts with the phenyl group of 3FPBA in the sp^2 form via cation-π interactions.

Next, we discuss the effect of Glc on the chemical shifts of 3FPBA with CTAB. In the presence of 10 mM CTAB and 200 mM Glc in ^{11}B NMR, a signal appears at 8.4 ppm (**Figure 9d**). This signal originates in the sp^3 boron[46]. Under identical conditions in the ^{19}F NMR, a signal appears at −40.2 ppm, and the signal at −38.8 ppm becomes smaller (**Figure 9h**). This result shows that the sp^3 hybridized boron increases, whereas the sp^2 hybridized boron decreases. The signal at −40.2 ppm in **Figure 9h** is consistent with the signal derived from sp^3 hybridized boron in the presence of 200 mM Glc (**Figure 9f**). Thus, this result suggests that 3FPBA exists as the sp^3 hybridized boron bound to Glc, with no interaction with CTAB. To further demonstrate this observation, we added the ^{11}B and ^{19}F NMR results of 10 mM 3FPBA and 10 mM CTAB at

various Glc concentrations (**Figure S5**). In ^{11}B NMR, signal detection in the spectra with 6.25–100 mM Glc was indeterminate (**Figures S5a–e**). Under identical conditions in the ^{19}F NMR, a signal at −40.1 ppm originating from the sp^3 boron was detected in the presence of 6.25 mM Glc. The signal became larger with an increase in the Glc concentration (**Figures S5f–j**). We observed that the sp^3 hybridized boron was detected despite the concentration of Glc (6.25 mM) being lower than that of 3FPBA (10 mM). This understanding is useful for explaining the viscosity change shown in **Figure 5**. Even if the concentration of Glc (below 40 mM) was lower than that of 3FPBA (60 mM), sp^3 hybridized boron was formed, which caused a decrease in the viscosity of the WLMs.

In addition, we studied the effect of other polyols (Pen, Man, Gal, or Fru) on the chemical shifts of 3FPBA in the presence of CTAB. We could not assess the reactivity of 3FPBA toward polyols using ^{11}B NMR spectra because the sp^2 boron signal disappeared in the presence of CTAB (**Figures S6a–d)**. In contrast, the ^{19}F NMR spectra presented two types of signals, which were ascribed to the sp^2 and sp^3 boron atoms, even in the presence of CTAB, and the balance between the sp^2 and sp^3 boron atoms could be used to assess the reactivity of 3FPBA toward polyols (**Figures S6e, f**). As illustrated in **Figures 9g and h**, Glc induced the conversion of sp^2 boron (−39 ppm) to sp^3 boron (−40 ppm). Pen, Man, Gal and Fru induced larger conversions than Glc. The signal of sp^2 boron was weak in the presence Gal and Pen, and disappeared in the presence Man and Fru (**Figures S6e–h**). This trend was in agreement with the reactivity of PBA toward polyols,[34,37] which is as follows: Fru > Man > Pen > Gal > Glc. This result demonstrated that 3FPBA was reactive toward polyol even in the presence of CTAB. This polyol selectivity study also revealed that ^{19}F NMR analysis could be used to evaluate the reactivity of 3FPBA toward polyol when ^{11}B NMR was ineffective.

3.5. Mechanism of formation and polyol-induced deformation of WLMs

We demonstrated that at pH 7.4, the formation of the WLM structure in System 1 exhibited high viscoelasticity. From a micro perspective, the cation-π interactions between the phenyl group of 3FPBA and the quaternary ammonium ion of CTAB was confirmed using ^{19}F and ^{1}H NMR (**Figures 9e and g and 10**). Such interactions have been previously reported, not only in ^{19}F NMR[47] but also in ^{1}H NMR[50–52]. Moreover, ^{19}F NMR demonstrates that at pH 7.4, 3FPBA mainly exists in molecular form (**Figures 8d** and **9e**). From these results, we propose that the 3FPBA of the sp^2 hybridized form is inserted on the surface of the CTAB micelles through cation-π interactions and WLMs are formed. **Figure 11a** shows the proposed schematic diagrams for the formation of WLMs.

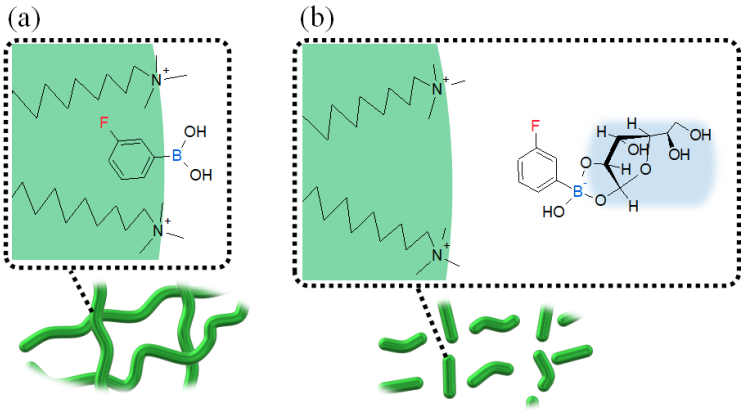

Figure 11. Proposed schematic diagram for the formation of worm-like micelles (WLMs) in System 1 (a), and the deformation of WLMs by adding Glc (b).

We demonstrate a decrease in the viscosity of System 1, depending on the polyol concentration, except for DEG (**Figures 2a** and **5**). In the Cole-Cole plot, Glc deviates from the perfect semicircular plot (**Figure S2b**). This result suggests that Glc partially breaks the structure of the WLMs. In addition, Glc lowers the τ of System 1 in dynamic viscoelasticity studies (**Figure 7**), which means that the chain of the WLMs is shortened when Glc is added. The results of the ^{19}F NMR reveal that the sp^3 hybridized boron of 3FPBA increases, whereas that of the sp^2 hybridized boron decreases upon the addition of Glc (**Figure 9g, h and Figures S5f-j**) or polyol (**Figure S6e-h**). Moreover, ^{19}F NMR indicates that the 3FPBA of the sp^3 hybridized boron bound to Glc does not interact with CTAB (**Figure 9f, h**). We propose the mechanism of the polyol response as follows: In the presence of polyol, the sp^3 hybridized boron of 3FPBA increases, whereas the sp^2 hybridized boron decreases. This change means that the structural component of the WLM decreases, which induces the disruption of the WLMs and decreases the viscosity (**Figure 11b**). These formation and deformation mechanisms of the WLMs are noticeable because it is commonplace that CTAB interacts with anionic aromatic compounds such as sodium salicylate to form WLMs.[6,7,10,16] However, in the case of 3FPBA with CTAB, the neutral form of 3FPBA (sp^2 boron), and not the anionic form (sp^3 boron), interacts with CTAB to form WLMs at pH 7.4. Moreover, the anionic form of 3FPBA (sp^3 boron), which binds to polyols, does not interact with CTAB, leading to deformation of the WLMs. Without ^{19}F NMR measurements, this insight would not be found.

4. CONCLUSIONS

To investigate the behavior of the WLMs at the molecular level, we successfully utilized ^{19}F NMR data by selecting fluorinated PBA as a component of the WLMs. We conclude that the driving force for the formation of WLMs is the cation-π interaction between the sp^2 hybrid of 3FPBA and the quaternary ammonium ion of CTAB. In addition, we reveal the mechanisms of the polyol-induced deformation of WLMs. With the addition of polyol, 3FPBA changes from a neutral to an anionic form. This change leads to the disruption of the WLMs, where the WLMs exhibit polyol-responsiveness. These mechanisms could not be elucidated by using the ^{11}B NMR exclusively with PBA derivatives in the absence of fluorine. We propose a unique concept that the change in the molecular state of PBA derivatives by adding polyol induces the deformation of WLMs and decreases the viscosity. This understanding of the WLMs at the molecular level will contribute to the further development of polyol-responsive WLMs using PBA derivatives.

ASSOCIATED CONTENT

Supporting Information

Steady viscosity behavior, Cole–Cole plot, UV spectra, relationship between pH and absorbance, ^{11}B and ^{19}F NMR spectra (PDF).

REFERENCES

(1) Hennink, W. E.; van Nostrum, C. F. Novel Crosslinking Methods to Design Hydrogels. *Adv. Drug Deliv. Rev.* **2012**, *64*, 223–236.

(2) Lau, H. K.; Kiick, K. L. Opportunities for Multicomponent Hybrid Hydrogels in Biomedical Applications. *Biomacromolecules* **2015**, *16*, 28–42.

(3) Segarra-Maset, M. D.; Nebot, V. J.; Miravet, J. F.; Escuder, B. Control of Molecular Gelation by Chemical Stimuli. *Chem. Soc. Rev.* **2013**, *42*, 7086–7098.

(4) Ikeda, M. Stimuli-Responsive Supramolecular Systems Guided by Chemical Reactions. *Polym. J.* **2019**, *51*, 371–380.

(5) Chu, Z.; Dreiss, C. A.; Feng, Y. Smart Wormlike Micelles. *Chem. Soc. Rev.* **2013**, *42*, 7174–7203.

(6) Shikata, T.; Hirata, H. Micelle Formation of Detergent Molecules in Aqueous Media: Viscoelastic Properties of Aqueous Cetyltrimethylammonium Bromide Solutions. *Langmuir* **1987**, *3*, 1081–1086.

(7) Shikata, T.; Hirata, H.; Kotaka, T. Micelle Formation of Detergent Molecules in Aqueous Media. 2. Role of Free Salicylate Ions on Viscoelastic Properties of Aqueous Cetyltrimethylammonium Bromide-Sodium Salicylate Solutions. *Langmuir* **1988**, *4*, 354–359.

(8) Chu, Z.; Dreiss, C. A.; Feng, Y. Smart Wormlike Micelles. *Chem. Soc. Rev.* **2013**, *42*, 7174.

(9) Sakai, H.; Orihara, Y.; Kodashima, H.; Matsumura, A.; Ohkubo, T.; Tsuchiya, K.; Abe, M. Photoinduced Reversible Change of Fluid Viscosity. *J. Am. Chem. Soc.* **2005**, *127*, 13454–13455.

(10) Ketner, A. M.; Kumar, R.; Davies, T. S.; Elder, P. W.; Raghavan, S. R. A Simple Class of Photorheological Fluids: Surfactant Solutions with Viscosity Tunable by Light. *J. Am. Chem. Soc.* **2007**, *129*, 1553–1559.

(11) Akamatsu, M.; Shiina, M.; Shrestha, R. G.; Sakai, K.; Abe, M.; Sakai, H. Photoinduced Viscosity Control of Lecithin-Based Reverse Wormlike Micellar Systems Using Azobenzene Derivatives. *RSC Adv.* **2018**, *8*, 23742–23747.

(12) Zhao, M.; Gao, M.; Dai, C.; Zou, C.; Yang, Z.; Wu, X.; Liu, Y.; Wu, Y.; Fang, S.; Lv, W. Investigation of Novel Triple-Responsive Wormlike Micelles. *Langmuir* **2017**, *33*, 4319–4327.

(13) Davies, T. S.; Ketner, A. M.; Raghavan, S. R. Self-Assembly of Surfactant Vesicles That Transform into Viscoelastic Wormlike Micelles upon Heating. *J. Am. Chem. Soc.* **2006**, *128*, 6669–6675.

(14) Tsuchiya, K.; Orihara, Y.; Kondo, Y.; Yoshino, N.; Ohkubo, T.; Sakai, H.; Abe, M. Control of Viscoelasticity Using Redox Reaction. *J. Am. Chem. Soc.* **2004**, *126*, 12282–12283.

(15) Sugai, J.; Saito, N.; Takahashi, Y.; Kondo, Y. Synthesis and Viscoelastic Properties of Gemini Surfactants Containing Redox-Active Ferrocenyl Groups. *Colloids Surf. A Physicochem. Eng. Asp.* **2019**, *572*, 197–202.

(16) Lin, Y.; Han, X.; Huang, J.; Fu, H.; Yu, C. A Facile Route to Design pH-Responsive Viscoelastic Wormlike Micelles: Smart Use of Hydrotropes. *J. Colloid Interface Sci.* **2009**, *330*, 449–455.

(17) Huang, Q.; Wang, L.; Yu, H.; Ur-Rahman, K. Advances in Phenylboronic Acid-Based Closed-Loop Smart Drug Delivery System for Diabetic Therapy. *J. Control. Release* **2019**, *305*, 50–64.

(18) Wang, J.; Wang, Z.; Yu, J.; Kahkoska, A. R.; Buse, J. B.; Gu, Z. Glucose-Responsive Insulin and Delivery Systems: Innovation and Translation. *Adv. Mater.* **2019**, 1902004.

(19) Sun, X.; James, T. D. Glucose Sensing in Supramolecular Chemistry. *Chem. Rev.* **2015**, *115*, 8001–8037.

(20) Dufort, B. M.; Tibbitt, M. W. Design of Moldable Hydrogels for Biomedical Applications Using Dynamic Covalent Boronic Esters. *Mater. Today Chem.* **2019**, *12*, 16–33.

(21) Mo, R.; Jiang, T.; Di, J.; Tai, W.; Gu, Z. Emerging Micro- and Nanotechnology Based Synthetic Approaches for Insulin Delivery. *Chem. Soc. Rev.* **2014**, *43*, 3595–3629.

(22) Patenall, B. L.; Williams, G. T.; Gwynne, L.; Stephens, L. J.; Lampard, E. V.; Hathaway, H. J.; Thet, N. T.; Young, A. E.; Sutton, M. J.; Short, R. D.; Bull, S. D.; James, T. D.; Sedgwick, A. C.; Jenkins, A. T. A. Reaction-Based Indicator Displacement Assay (RIA) for the Development of a Triggered Release System Capable of Biofilm Inhibition. *Chem. Commun.* **2019**, *55*, 15129–15132.

(23) Williams, G. T.; Sedgwick, A. C.; Sen, S.; Gwynne, L.; Gardiner, J. E.; Brewster, J. T.; Hiscock, J. R.; James, T. D.; Jenkins, A. T. A.; Sessler, J. L. Boronate Ester Cross-Linked PVA Hydrogels for the Capture and H_2O_2-Mediated Release of Active Fluorophores. *Chem. Commun.* **2020**, *56*, 5516–5519.

(24) Lampard, E. V.; Sedgwick, A. C.; Sombuttan, T.; Williams, G. T.; Wannalerse, B.; Jenkins, A. T. A.; Bull, S. D.; James, T. D. Dye Displacement Assay for Saccharides Using Benzoxaborole Hydrogels. *ChemistryOpen* **2018**, *7*, 266–268.

(25) Xu, S.; Sedgwick, A. C.; Elfeky, S. A.; Chen, W.; Jones, A. S.; Williams, G. T.; Jenkins, A. T. A.; Bull, S. D.; Fossey, J. S.; James, T. D. A Boronic Acid-Based Fluorescent Hydrogel for Monosaccharide Detection. *Front. Chem. Sci. Eng.* **2020**, *14*, 112–116.

(26) Miki, R.; Takei, C.; Ohtani, Y.; Kawashima, K.; Yoshida, A.; Kojima, Y.; Egawa, Y.; Seki, T.; Iohara, D.; Anraku, M.; Hirayama, F.; Uekama, K. Glucose Responsive Rheological Change and Drug Release from a Novel Worm-like Micelle Gel Formed in Cetyltrimethylammonium Bromide/Phenylboronic Acid/Water System. *Mol. Pharm.* **2018**, *15*, 1097–1104.

(27) London, R. E.; Gabel, S. A. Fluorine-^{19} NMR Studies of Fluorobenzeneboronic Acids. 1. Interaction Kinetics with Biologically Significant Ligands. *J. Am. Chem. Soc.* **1994**, *116*, 2562–2569.

(28) Mikkelsen, K.; Nielsen, S. O. Acidity Measurements with the Glass Electrode in H_2O-D_2O Mixtures. *J. Phys. Chem.* **1960**, *64*, 632–637.

(29) Krężel, A.; Bal, W. A Formula for Correlating pK_a Values Determined in D_2O and H_2O. *J. Inorg. Biochem.* **2004**, *98*, 161–166.

(30) Shrestha, R. G.; Shrestha, L. K.; Aramaki, K. Formation of Wormlike Micelle in a Mixed Amino-Acid Based Anionic Surfactant and Cationic Surfactant Systems. *J. Colloid Interface Sci.* **2007**, *311*, 276–284.

(31) Varade, D.; Sharma, S. C.; Aramaki, K. Viscoelastic Behavior of Surfactants Worm-like Micellar Solution in the Presence of Alkanolamide. *J. Colloid Interface Sci.* **2007**, *313*, 680–685.

(32) Zhao, Y.; Haward, S. J.; Shen, A. Q. Rheological Characterizations of Wormlike Micellar Solutions Containing Cationic Surfactant and Anionic Hydrotropic Salt. *J. Rheol.* **2015**, *59*, 1229–1259.

(33) Wang, P.; Kang, W.; Yang, H.; Zhao, Y.; Yin, X.; Zhu, Z.; Zhang, X. The *N*-Allyl Substituted Effect on Wormlike Micelles and Salt Tolerance of a C_{22}-Tailed Cationic Surfactant. *Soft Matter* **2017**, *13*, 7425–7432.

(34) Springsteen, G.; Wang, B. A Detailed Examination of Boronic Acid–Diol Complexation. *Tetrahedron* **2002**, *58*, 5291–5300.

(35) Wu, X.; Li, Z.; Chen, X. X.; Fossey, J. S.; James, T. D.; Jiang, Y. B. Selective Sensing of Saccharides Using Simple Boronic Acids and Their Aggregates. *Chem. Soc. Rev.* **2013**, *42*, 8032–8048.

(36) Matsushima, Y.; Nishiyabu, R.; Takanashi, N.; Haruta, M.; Kimura, H.; Kubo, Y. Boronate Self-Assemblies with Embedded Au Nanoparticles: Preparation, Characterization and Their Catalytic Activities for the Reduction of Nitroaromatic Compounds. *J. Mater. Chem.* **2012**, *22*, 24124–24131.

(37) Lorand, J. P.; Edwards, J. O. Polyol Complexes and Structure of the Benzeneboronate Ion. *J. Org. Chem.* **1959**, *24*, 769–774.

(38) Khatory, A.; Lequeux, F.; Kern, F.; Candau, S. J. Linear and Nonlinear Viscoelasticity of Semidilute Solutions of Wormlike Micelles at High Salt Content. *Langmuir* **1993**, *9*, 1456–1464.

(39) Wang, P.; Tan, J.; Pei, S.; Wang, J.; Zhang, Y.; Sun, X.; Zhang, J. Dual Effects of Cationic Surfactant on the Wormlike Micelle Formation of Catanionic Surfactants Mixtures: An Experiment and Simulation Study. *Colloids Surf. A Physicochem. Eng. Asp.* **2017**, *529*, 95–101.

(40) Bi, Y.; Wei, H.; Hu, Q.; Xu, W.; Gong, Y.; Yu, L. Wormlike Micelles with Photoresponsive Viscoelastic Behavior Formed by Surface Active Ionic Liquid/Azobenzene Derivative Mixed Solution. *Langmuir* **2015**, *31*, 3789–3798.

(41) Cates, M. E.; Candau, S. J. Statics and Dynamics of Worm-like Surfactant Micelles. *J. Phys. Condens. Matter* **1990**, *2*, 6869–6892.

(42) Hashizaki, K.; Taguchi, H.; Saito, Y. A Novel Reverse Worm-like Micelle from a Lecithin/Sucrose Fatty Acid Ester/Oil System. *Colloid Polym. Sci.* **2009**, *287*, 1099–1105.

(43) Axthelm, J.; Görls, H.; Schubert, U. S.; Schiller, A. Fluorinated Boronic Acid-Appended Bipyridinium Salts for Diol Recognition and Discrimination via ^{19}F NMR Barcodes. *J. Am. Chem. Soc.* **2015**, *137*, 15402–15405.

(44) Iannazzo, L.; Benedetti, E.; Catala, M.; Etheve-Quelquejeu, M.; Tisné, C.; Micouin, L. Monitoring of Reversible Boronic Acid-Diol Interactions by Fluorine NMR Spectroscopy in Aqueous Media. *Org. Biomol. Chem.* **2015**, *13*, 8817–8821.

(45) Axthelm, J.; Askes, S. H. C.; Elstner, M.; G, U. R.; Görls, H.; Bellstedt, P.; Schiller, A. Fluorinated Boronic Acid-Appended Pyridinium Salts and ^{19}F NMR Spectroscopy for Diol Sensing. *J. Am. Chem. Soc.* **2017**, *139*, 11413–11420.

(46) Stolowitz, M. L.; Ahlem, C.; Hughes, K. A.; Kaiser, R. J.; Kesicki, E. A.; Li, G.; Lund, K. P.; Torkelson, S. M.; Wiley, J. P. Phenylboronic Acid−Salicylhydroxamic Acid Bioconjugates. 1. A Novel Boronic Acid Complex for Protein Immobilization. *Bioconjug. Chem.* **2001**, *12*, 229–239.

(47) Vermathen, M.; Stiles, P.; Bachofer, S. J.; Simonis, U. Investigations of Monofluoro-Substituted Benzoates at the Tetradecyltrimethylammonium Micellar Interface. *Langmuir* **2002**, *18*, 1030–1042.

(48) Broxton, T. J.; Christie, J. R.; Chung, R. P. T. Micellar Catalysis of Organic Reactions. 23. Effect of Micellar Orientation of the Substrate on the Magnitude of Micellar Catalysis. *J. Org. Chem.* **1988**, *53*, 3081–3084.

(49) Kumar, S.; Sharma, D. Role of Partitioning Site in Producing Viscoelasticity in Micellar Solutions. *J. Surfactants Deterg.* **2005**, *8*, 247–252.

(50) Sabatino, P.; Szczygiel, A.; Sinnaeve, D.; Hakimhashemi, M.; Saveyn, H.; Martins, J. C.; Van der Meeren, P. NMR Study of the Influence of pH on Phenol Sorption in Cationic CTAB Micellar Solutions. *Colloids Surf. A Physicochem. Eng. Asp.* **2010**, *370*, 42–48.

(51) Groth, C.; Nydén, M.; Cecilia Persson, K. Interactions between Benzyl Benzoate and Single- and Double-Chain Quaternary Ammonium Surfactants. *Langmuir* **2007**, *23*, 3000–3008.

(52) Chaghi, R.; de Ménorval, L. C.; Charnay, C.; Derrien, G.; Zajac, J. Interactions of Phenol with Cationic Micelles of Hexadecyltrimethylammonium Bromide Studied by Titration Calorimetry, Conductimetry, and ^{1}H NMR in the Range of Low Additive and Surfactant Concentrations. *J. Colloid Interface Sci.* **2008**, *326*, 227–234.

A graphic for the "Table of Contents"